Modeling and experimental electro-optic response of dielectric lithium niobate waveguides used as electric field sensors

Modeling and experimental electro-optic response of dielectric lithium niobate waveguides used as electric field sensors

C Gutiérrez-Martínez[1]**, J Santos-Aguilar, R Ochoa-Valiente, M Santiago-Bernal and A Morales-Díaz**

Instituto Nacional de Astrofísica, Óptica y Electrónica (INAOE), Apdo Postal 51, 72000 Puebla, Pue., Mexico

E-mail: cgutz@inaoep.mx

Abstract

In this paper, the static optical transfer function of dielectric lithium niobate ($LiNbO_3$) electro-optic sensors is modeled and experimentally measured. This function represents the transmitted optical power at the output of an optical waveguide in a $LiNbO_3$ crystal which acts as an electric field sensor. The sensor is electrode-less and operates as a dielectric probe. Under such a condition, the electric field is present in the dielectric media surrounding the waveguide and the measured field intensity is determined by the boundary condition between the media and the $LiNbO_3$ crystal. The electro-optic transfer function is theoretically modeled and experimentally measured. Such a transfer function shows a sinusoidal shape, from which the half-wave electric field, the optical extinction ratio and the linear and nonlinear regions can be determined. $LiNbO_3$ electric field sensors are inherently wide band, and a sensing scheme is tested, showing a high-linearity sensing detection of high-intensity and wide-band electric fields.

Keywords: $LiNbO_3$ crystals, electro-optic sensors, polarization interferometers, static optical function transfer, electric field sensing

1. Introduction

Electric field measurement is an important subject in scientific, industrial or commercial environments. Static and dynamic electric fields are generated by different sources including natural lightning and strokes, electric power equipment, power generation and distribution facilities, high-voltage transmission lines, telecommunication equipments, electromagnetic interference, human medical signals, etc. Very often, electric field meters use conductive electrodes, which are interconnected by cables to the measuring electronics, but such arrangements easily distort the observed fields. Different techniques and apparatus for the measurement of electric fields are reported in the technical literature, for instance, measurement of ac and dc electric fields in high-voltage transmission lines using fluorescent tubes and electro-

mechanical field mills; human electroencephalograms are recorded using sensitive electric field sensors in the form of probe electrode disks to characterize brain activity [1–7]. The most common method for measuring atmospheric fields is based on the field mill, which consists of a set-up based on fixed and rotating plates. The measured electric field induces an electric charge on a fixed plate. The sensing electrode is a rotating plate, which is alternatively exposed and shielded from the induced charge, thus showing an alternating charge on it. The sensed charge is converted into either an alternating current or voltage. A very nice explanation of such a process is given in [4]. Some commercial devices are based on the field mill method [6, 7].

An alternative approach for sensing electric fields consists in using light instead of electrical methods. In this case, light senses and is modulated by the electric field while traveling through an electro-optic material, taking advantage of the Pockels effect. As the optical techniques minimally disturb

[1] Author to whom any correspondence should be addressed.

the electric field and are inherently immune to electromagnetic interference, a wide variety of sensing schemes using optical fibers and electro-optic devices has been reported over several years [8–18].

Most of such schemes use the Pockels effect on lithium niobate (LiNbO$_3$) electro-optic waveguides. Sensor devices either using electrodes or no electrodes have been studied and integrated with different experimental schemes. Using electrodes in the sensing devices gives a high sensitivity, but the main disadvantage is that they may disturb the measured electric field. Such schemes are very well adapted to measure low-intensity electric fields (mV m^{-1} to hundreds V m^{-1}) as found in telecommunication systems and electronic apparatus. Electrode-less sensors minimally disturb the measured field, but the sensitivity is relatively lower and such devices are better adapted to the measurement of high-intensity electric fields ranging from some kV m^{-1} to hundreds of kV m^{-1} (1 to 2000 kV m^{-1}), as found in natural lightning strikes, high power electrical facilities and high-voltage transmission lines.

Electric field sensing schemes using optical techniques based on fiber optics and electrode-less electro-optic lithium niobate (LiNbO$_3$) crystals are being studied [14–18]. The electro-optic sensors are integrated with sensing schemes which can be configured either as polarization or Mach-Zehnder optical interferometers. In any case, the optical transfer function of the electro-optic sensor must be determined, as such a characteristic defines the linear and nonlinear sensing ranges. The transfer function showing a sinusoidal shape also determines the half-wave electric field and the optical extinction ratio.

The model of the static optical transfer function of LiNbO$_3$ waveguides, used as dielectric (electrode-less) electric field sensors, and the experimental characterization are reported in this paper. Even if this subject may seem obvious, it has been scarcely analyzed in the technical literature as related to electro-optic sensors. In this paper, the static optical transfer function is modeled by sensing a high-intensity electric field, which modulates an optical beam traveling through an optical waveguide which is a component of an integrated optics polarization interferometer. The optical transfer function is a fundamental response, as it determines the ranges where electric field can be linearly sensed and measured.

In this paper, three complementary steps are described. In the first step, the mathematical model for the optical transfer function of the LiNbO$_3$ electro-optic sensor is proposed. Such a model allows calculating the transmitted optical transfer function depending on the sensed electric field. This response shows a cosinusoidal shape and the distance between the maximum and minimum transmitted optical powers corresponds to the half-wave electric field E_π.

In the second step, for validating the theoretical analysis, an automated experimental set-up is proposed for measuring the electro-optic function transfer. In such a set-up, an electric field is generated by applying a high voltage to a set of parallel plates, which are not in contact with the optical waveguides. The parallel plates generate a uniform electric field and the filling dielectrics are an air layer and the LiNbO$_3$ crystal. The electro-optic transfer function is measured and compared
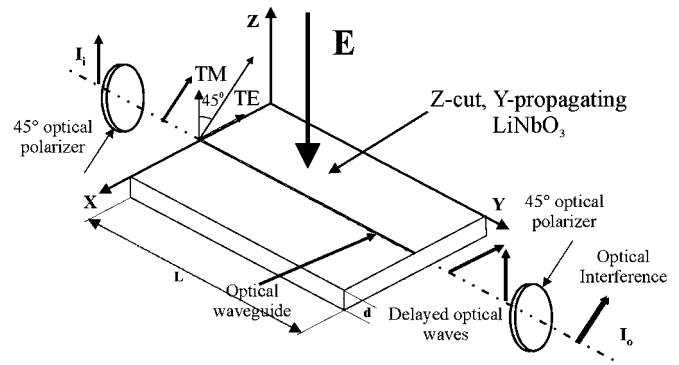

Figure 1. A LiNbO$_3$ polarization interferometer.

to the theoretical model. The electric field sensor is an optical waveguide on the surface of a 1 mm thick LiNbO$_3$ crystal. In the experimental set-up, the optical waveguide acts as a polarization interferometer and the sensed electric field modulates the transmitted optical intensity.

In the third step, one of the characterized electro-optic sensors is used to implement an electric field sensing scheme, based on the polarization interferometer. The sensing scheme of wide-band ac electric fields of 20–90 kVpp m^{-1}, in a band of 0–100 kHz, is described. The sensing scheme is adjusted around the quadrature point of the first linear electro-optic sensing region and a linear sensing-detection process is achieved.

The use of LiNbO$_3$ electro-optic sensors is also attractive for wide-band sensing schemes, based on the high frequency response of such devices, reaching potentially up to several GHz. Sensing wide-band electric fields is currently a potential application in optoelectronic instrumentation, aiming to measure static and dynamic electric fields in electric power equipment, generation and distribution of electrical power, telecommunication equipment and facilities, medical applications, etc.

2. Modeling the electro-optic transfer function of a LiNbO$_3$ electro-optic sensor

LiNbO$_3$ is an electro-optic birefringent material that can be used either as optical modulator or as an electric field sensor.

A simple electric field sensing scheme can be configured based on a polarization interferometer, as realized when a LiNbO$_3$ optical waveguide is placed between 45° crossed light polarizers [19]. Such a basic scheme is depicted in figure 1.

The electro-optic sensor is an optical waveguide on a Z-cut, Y-propagating LiNbO$_3$ crystal of length L (mm) and thickness d (mm). In a polarization interferometer, light coming from an optical source is firstly polarized at 45° relative to the X and Z optical axes. This launched light then propagates in its transverse-electric (TE) and transverse-magnetic (TM) orthogonal modes, at different velocities as determined by the ordinary and extra-ordinary refractive indices. At the output of the optical waveguide, the optical modes are delayed and a second polarizer at 45° re-orientates them for ensuring
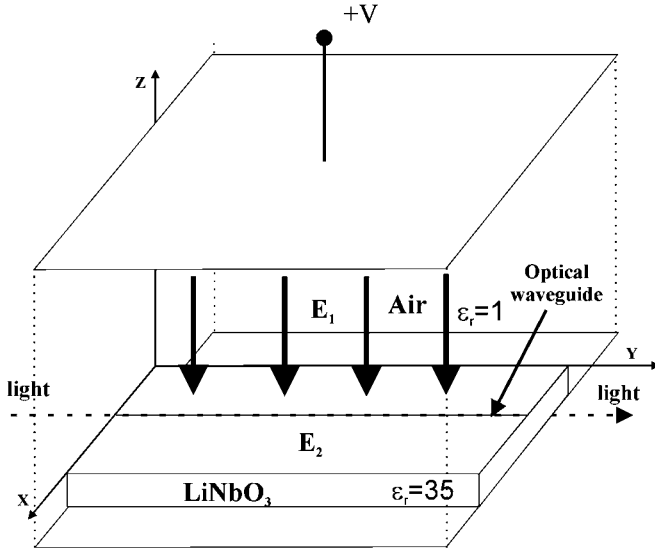
Figure 2. Dielectric electric field sensor.

interference. The output of the polarization interferometer can be detected as an optical intensity.

When an electric field (E) is sensed by the optical waveguide, the photo-detected optical intensity at the output of the polarization interferometer is given as

$$I_o(E) = \frac{I_i}{2} - \frac{I_i}{2} \cos\left(\varphi_0 - \pi \frac{E}{E_\pi}\right) \quad (1)$$

where the static optical phase difference introduced by the length L of crystal is $\phi_0 = \frac{2\pi}{\lambda_0}(n_o - n_e)L$. The half-wave electric field, which switches the output optical intensity between its maximum and minimum values, is given as

$$E_\pi = \frac{\lambda_0}{\left(r_{33}n_e^3 \Gamma_{TM} - r_{13}n_o^3 \Gamma_{TE}\right)L} \quad (2)$$

where λ_0 is the center wavelength of the light beam; n_o and n_e are the refractive indices for the ordinary and extraordinary axis respectively; r_{33} and r_{13} are the Pockels coefficients of LiNbO$_3$; Γ_{TE} and Γ_{TM} are the optical-electrical overlapping integrals.

Equation (1) represents the optical transfer function and it depends mainly on a static phase parameter and on the sensed electric field.

When the optical waveguide is used as a dielectric sensor, no electrodes are associated with the crystal and the electric field is present in the dielectric environment (most commonly air, $\varepsilon_r = 1$), surrounding the LiNbO$_3$ crystal.

To generate a high-intensity electric field, an experimental set-up was proposed, figure 2. The electric field was generated by applying a high voltage to a set of parallel metallic plates. The electro-optic sensor was placed between the plates, but not in contact with them, as an air layer of thickness (d_{air}) separates the upper plate from the LiNbO$_3$ crystal of thickness (d_{LiNbO_3}). As the plates are wide enough ($\geqslant 20$ mm) and the optical waveguide is 10 μm wide, the sensed electric field is uniform in the waveguide.

As illustrated in figure 2, the electric field in the air E_1, finds a boundary condition on the surface of the electro-optic

Table 1. Static parameters of LiNbO$_3$ electric field sensors.

L (mm)	φ_0 (rad)	E_π (kV m^{-1})
5	1918	868
10	3837	434
30	11 511	144
60	23 022	72

sensor. The discontinuity is determined by the permittivities of the air ($\varepsilon_r = 1$) and of crystal ($\varepsilon_r = 35$), respectively. The applied voltage between the parallel plates is divided on the air layer and on the LiNbO$_3$ crystal as $V = V_{air} + V_{LiNbO_3}$.

The electric field across the electro-optic crystal is [20]

$$E_2 = \frac{V_{LiNbO_3}}{d_{LiNbO_3}}. \quad (3)$$

As the electric field is perpendicular to the crystal surface and considering the boundary conditions between two dielectric media, the relationship between the normal electric fields is $\varepsilon_{r_1} E_1 = \varepsilon_{r_2} E_2$.

In the optical waveguide, the sensed electric field E_2 is given as

$$E_2 = \frac{\varepsilon_{r_1}}{\varepsilon_{r_2}} E_1. \quad (4)$$

The sensed electric field is 35 times weaker than the electric field in the air layer over the sensor surface. As light travels in the optical waveguide, it is modulated by the electric field. At the output of the optical waveguide, the optical transfer function is

$$T(E_2) = \frac{1}{2} - \frac{1}{2} \cos\left(\varphi_0 - \pi \frac{E_2}{E_\pi}\right). \quad (5)$$

Even if the sensed electric field varies linearly related to the external field E_1, as stated by equation (4), the modulated optical power varies as a cosine function of E_2, as given by equation (5). The electric field will be linearly sensed in different ranges around the quadrature points of the periodic electro-optic transfer function.

Figure 3 illustrates the theoretical electro-optic responses for 10, 30 and 60 mm long LiNbO$_3$ electric field sensors. The sensed electric field ranges between 0 and 850 kV m^{-1}. The optical transfer functions show the linear and nonlinear sensing ranges. From equation (2), E_π is calculated to be 434 kV m^{-1} for 10 mm; 144 kV m^{-1} for 30 mm and 72 kV m^{-1} for 60 mm crystals, respectively, at $\lambda_0 = 1310$ nm ($n_o = 2.2$ and $n_e = 2.14$).

After equations (2) and (5), the parameters φ_0 and the half-wave electric field E_π, for LiNbO$_3$ electro-optic sensors with $L = 10$, 30 and 60 mm at $\lambda_0 = 1310$ nm, are summarized in table 1.

3. Experimental optical transfer function

To validate the theoretical data, the electro-optical transfer functions for 12.9 and 36.5 mm long optical waveguides were measured using a polarization interferometer on an automated experimental setup, as shown in figure 4. The main
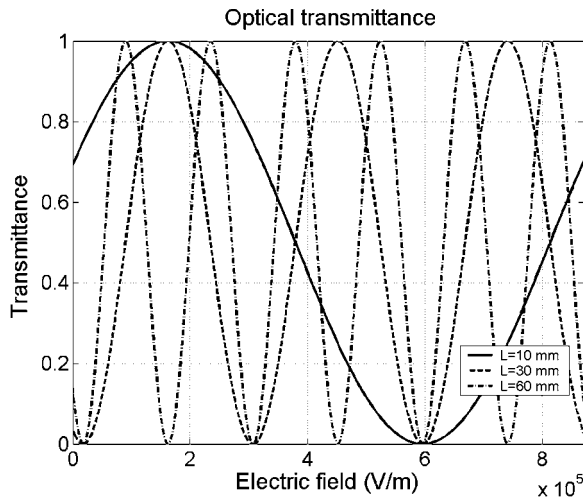
Figure 3. Theoretical optical transfer function of LiNbO$_3$ electro-optic sensors: $L = 10$, 30 and 60 mm.

components are a single mode laser diode (SML) emitting at 1310 nm, two 45° optical fiber polarizers, the LiNbO$_3$ sensor, a high-voltage dc source and a calibrated photo-detector/optical power meter. The voltage source and the power meter are computer controlled through a GPIB interface. The special-purpose software, for controlling the high-voltage power supply and the programmable optical power meter, has been developed in our laboratory. The program sweeps a high voltage on the set of parallel plates, in order to generate a testing uniform electric field. Light coming from the SML is injected into the sensing optical waveguide. The sensed electric field modulates the transmitted light and the optical transfer function is automatically measured.

An electric field was generated on the parallel plates and the test field E_2 was adjusted in a range of 0–850 kV m^{-1} so as to be sensed by the electro-optic crystals.

The optical transfer functions, for 12.9 and 36.5 mm long electro-optic sensors, are depicted in figures 5(*a*) and (*b*). In these figures, the theoretical and experimental optical transfer functions, in a linear scale, are displayed. The measured transfer functions are in good agreement with the theoretical prediction, as given by equation (2). From these curves, the theoretical (measured) half-wave electric field E_π is 333.8 kV m^{-1} (333.6 kV m^{-1}) for the 12.9 mm and

119.06 kV m^{-1} (120.5 kV m^{-1}) for the 36.5 mm sensors, respectively.

The optical transfer functions show the different linear sensing ranges dependent on the electric field intensities and on the length of the crystal, as can be observed in figures 5(*a*) and (*b*). For the 12.9 mm sensor, a first linear range is between 180 and 330 kV m^{-1}. A second linear range is between 540 and 580 kV m^{-1}. For the 36.5 mm sensor, a first linear sensing range is between 40 and 90 kV m^{-1}, a second one between 170 and 220 kV m^{-1}, and so on. From the graphs, it can be deduced that linear sensing is achieved when the sensor is biased at the quadrature points on the transfer function. In this way, when using the 12.9 mm sensor, linear sensing is achieved when biasing at a dc electric field of 280 kV m^{-1}. A second linear region is around 600 kV m^{-1}.

For the 36.5 mm sensor, four linear regions can be used. A first one when biasing the sensor around 60 kV m^{-1}, a second one around 190 kV m^{-1}, the third around 310 kV m^{-1} and a fourth one around 420 kV m^{-1}. For sensing in any of these regions, a bias static electric field must be applied in order to fix an operating point around the quadrature points of the transfer function. Once the operating point is fixed, the sensed electric field will modulate the transmitted optical intensity, giving transmittance values above or below the bias point, following the slope of the transfer function.

4. An electric field sensing scheme

To demonstrate a practical application, the previously characterized 36.5 mm long LiNbO$_3$ electro-optic sensor is integrated in a polarization interferometer electric field sensing setup, figure 6. A dynamic 0–100 kHz electric field is generated by a video high-voltage amplifier. In a previous work, a 20 kHz 'wide-band' electric field sensing scheme has been reported [21]. Sensing wide-band electric fields, at frequencies higher than 1 MHz, is an attractive application in industrial and commercial environments where high-intensity fields are present.

The optical transfer function of the 36.5 mm electro-optic sensor has been zoomed in the 0–225 kV m^{-1} range, as depicted in figure 7(*a*). In order to sense a dynamic electric field, a 50 kV m^{-1} biasing static field was fixed on the optical transfer function. Such a static field bias is provided by the high-voltage amplifier, whose output can fix a static dc voltage
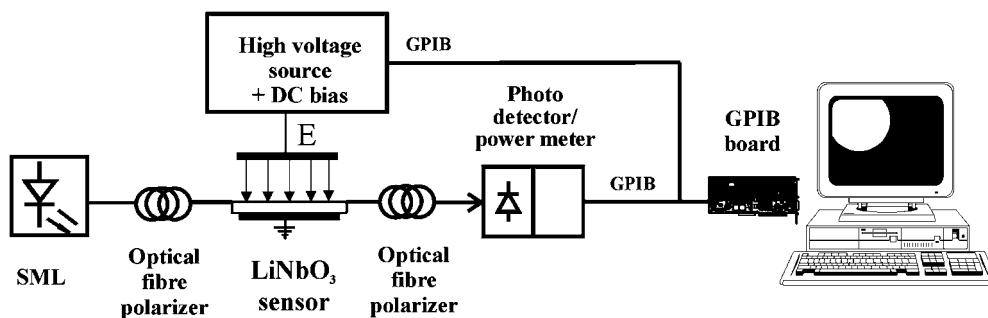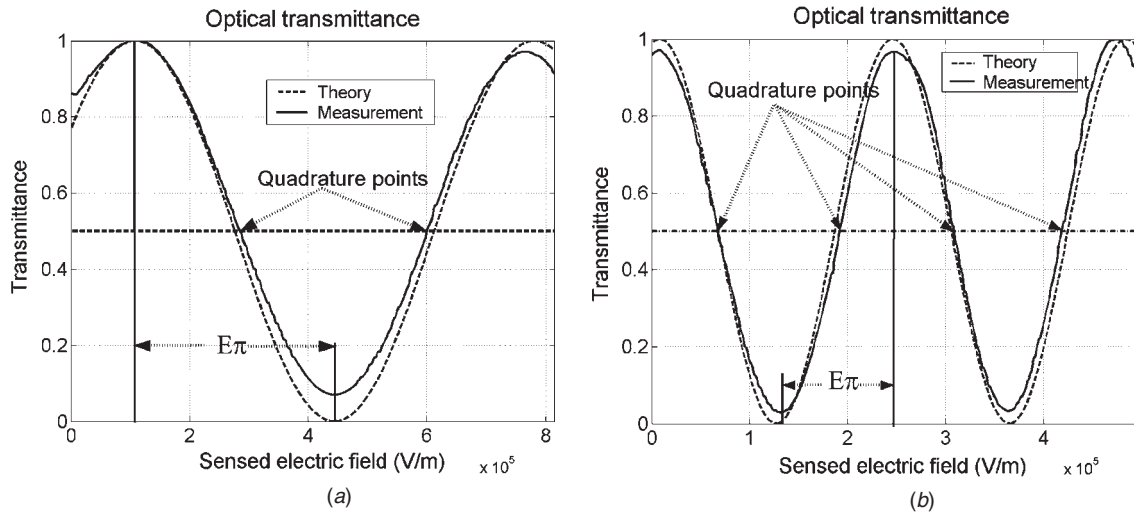

Figure 4. The automated characterization set-up.

Figure 5. Theoretical and measured optical transfer function of electro-optic sensors: (*a*) 12.9 mm; (*b*) 36.5 mm.
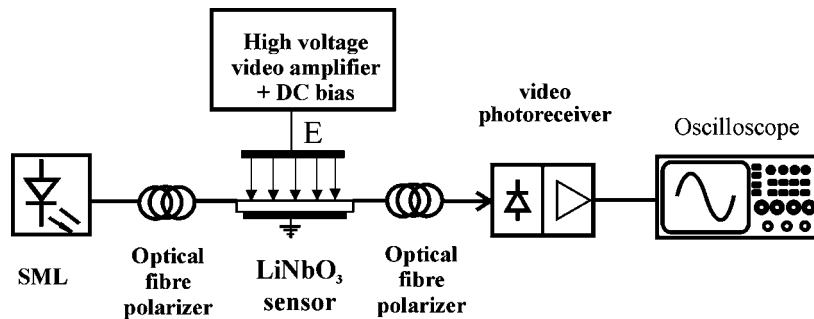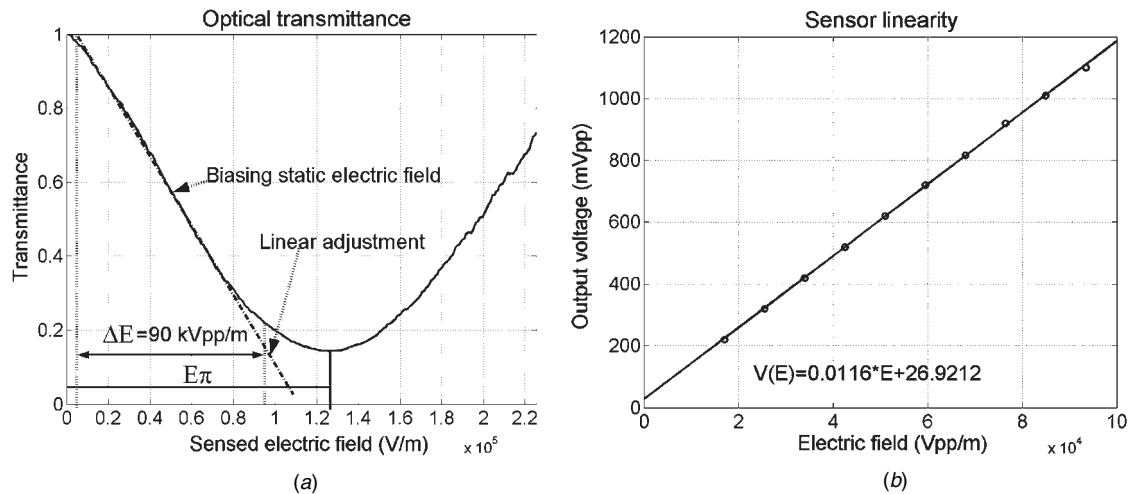

Figure 6. Wide-band electric field sensing set-up.

Figure 7. (*a*) The electro-optic transfer function of the 36.5 mm sensor 'zoomed' in a 0–225 kV m^{-1} range; (*b*) the linear response of the sensing scheme in 20–90 kVpp m^{-1} electric field range.

on the parallel plates. This dc voltage has been adjusted to generate a 50 kV m^{-1} static field operating point, as shown in figure 7(*a*). To test the sensing of ac electric fields, a 100 kHz dynamic electric field ranging between $\Delta E = 20$ and $\Delta E = 90$ kVpp m^{-1} was added to the biasing static electric field. The maximum deviation $\Delta E = 90$ kVpp m^{-1} represents 58% of E_π, and is located in the region where the transfer function is mostly linear, figure 7(*a*). In this figure, a reference straight line is fitted to the optical transfer function showing the

best adjustment of both curves. The sensing is linear between 10 and 90 kV m^{-1} on the horizontal axis.

After the optical transmission of the 100 kHz electric field, a homemade trans-impedance wide-band photo-receiver delivered a voltage proportional to the sensed electric field. The output voltage corresponding to 20 kVpp m^{-1} $\leqslant$ $\Delta E \leqslant 90$ kVpp m^{-1} electric field, is shown in figure 7(*b*). The dots represent the measured output voltages from the photo-receiver. The curve fitting of the output voltages from
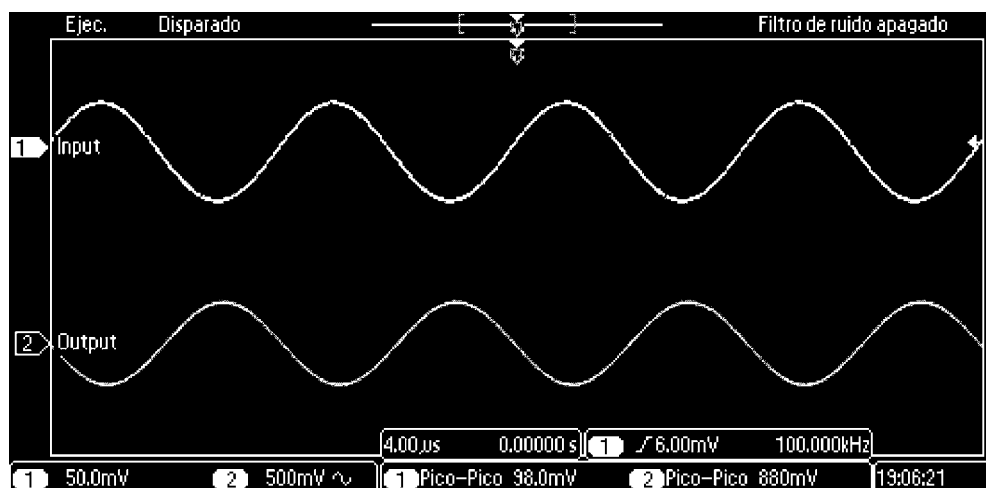
Figure 8. 100 kHz, 73.4 kVpp m^{-1} sensed ac electric field.

the photo-receiver in proportion to the sensed electric field is shown in this figure. The fitting straight line equation $V(E) = 0.0116 * E + 26.9212$ represents the calibration curve of the sensing scheme in the 20–90 kVpp m^{-1} range. From figure 7(*b*), it can be observed that the output voltage is highly linear to the sensed electric field, and the deviation from the straight line is really insignificant in this measurement range.

The measurement of an ac electric field of 73.4 kVpp m^{-1} (880 mVpp output signal) and 100 kHz is shown in figure 8. In this photograph, the upper waveform corresponds to the input to the wide-band amplifier; the lower waveform corresponds to the output voltage at the output of a video-band photo-receiver. The sensed electric field is recovered by an optimized trans-impedance photo-receiver where the noise is limited at 30 mVpp. For an output voltage of 880 mVpp, the signal-to-noise ratio is 30 dB. The scheme represents a promising technique as it shows a high-quality sensing–detection process (wide-band frequency response, high linearity and high signal-to-noise ratio). Work is in progress for optimizing a sensing scheme for detecting multi-MHz (video) electric fields.

5. Conclusions

In this paper, modeling of the theoretical optical transfer function of LiNbO$_3$ electric field sensors and the experimental validation are reported. The optical transfer function is a very important characteristic as it determines the linear and nonlinear operating regions depending on the sensed electric field intensity. The transfer functions of 12.9 and 36.5 mm electro-optic sensors were also experimentally measured and excellent agreement with the theoretical performance was found. To show a practical application of sensing electric fields, the 36.5 mm sensor was integrated in a sensing scheme and ac electric fields, in a band up to 1 MHz, were successfully measured. The sensing of a 100 kHz electric field has been demonstrated. The scheme exhibits a high linear response when adjusted for measuring ac electric fields in a range of 20–90 kV pp m^{-1} around a 50 kV m^{-1} static electric field bias. The experimental data match perfectly a straight line equation

after a curve fitting process. The measurements show a high signal-to-noise ratio of around 30 dB.

Work is in progress for detecting multi-MHz electric fields, taking advantage of the wide-band capabilities of LiNbO$_3$ electro-optic sensors.

References

[1] Johnston A R, Kirkham H and Eng B T 1986 DC electric field meter with fiber-optic readout *Rev. Sci. Instrum.* **57** 2746

[2] Kirkham H 2006 Measuring electric fields from power lines *IEEE Instrum. Meas. Magn.* **9** 54

[3] Kirkham H 2006 Measuring of electric fields generated from alternating current *IEEE Instrum. Meas. Magn.* **9** 58

[4] Kirkham H 2006 Dust devils and dust fountains: the measurement challenges *IEEE Instrum. Meas. Magn.* **9** 48

[5] Harland C J, Clark D T and Prance R J 2002 Remote detection of human electroencephalograms using ultrahigh input impedance electric potential sensors *Appl. Phys. Lett.* **81** 3284

[6] www.campbellsci.com/electric-fiels-sensor CS110, Electric Field Sensor, Campbell Scientific Inc. URL accessed on 12 January 2011

[7] www.missioninstruments.com/pages/products/efs1000.html Electric Field Mill Sensor EFS 1000 Series, Mission Instruments Corporation URL accessed on 12 January 2011

[8] Michie A, Bassett I M, Haywood J H and Ingram J 2007 Electric field and voltage sensing at 50 Hz using a thermally poled silica optical fibre *Meas. Sci. Technol.* **18** 3219

[9] Filippov V N, Starodumov A N, Barmenkov Y O and Makarov V V 2000 Fiber-optic voltage sensor based on a Bi$_{12}$TiO$_{20}$ crystal *Appl. Opt.* **39** 1389

[10] Meier T, Kostrzewa C, Petermann K and Schuppert B 1994 Integrated optical E-field probes with segmented modulator electrodes *IEEE J. Lightwave Technol.* **12** 1497

[11] Rao Y J, Gnewuch H, Pannell C N and Jackson D A 1999 Electro-optic electric field sensor based on periodically poled LiNbO$_3$ *Electron. Lett.* **35** 596

[12] Yim Y S, Shin S Y, Shay W T and Lee Ch T 1998 Lithium niobate integrated-optic voltage sensor with variable sensing ranges *Opt. Commun.* **152** 225

[13] Lee T H, Hwang F T, Shay W T and Lee Ch T 2006 Electromagnetic field sensor using Mach–Zehnder waveguide modulator *Microw. Opt. Technol. Lett.* **48** 1897

[14] Hidaka K and Fujita H 1982 A new method of electric field measurements in corona discharge using Pockels device *J. Appl. Phys.* **53** 5999–6003

[15] Naghski D H, Boyd J T, Jackson H E, Sriram S, Kingsley S A and Latess J 1994 An integrated photonic Mach–Zehnder interferometer with no electrodes for sensing electric fields *IEEE J. Lightwave Technol.* **12** 1092

[16] Cecelja F, Bordovsky M and Balachandran W 2001 Lithium niobate sensor for measurement of dc electric fields *IEEE Trans. Instrum. Meas.* **50** 465

[17] Cecelja F, Bordovsky M and Balachandran W 2001 Electro-optic sensor for measurement of dc fields in the presence of space charge *IEEE Trans. Instrum. Meas.* **51** 282

[18] Gutiérrez-Martínez C, Trinidad-Garcia G and Rodríguez-Asomoza J 2002 Electric field sensing system using coherence modulation of light *IEEE Trans. Instrum. Meas.* **51** 985

[19] Saleh B E A and Teich M C 1991 *Fundamentals of Photonics* (New York: Wiley)

[20] Ulaby F T 2000 *Fundamentals of Applied Electromagnetics* (Englewood Cliffs, NJ: Prentice-Hall)

[21] Gutiérrez-Martínez C, Santos-Aguilar J and Ochoa-Valiente R 2007 An all-fibre and integrated optics electric field sensing scheme using matched optical delays and coherence modulation of light *Meas. Sci. Technol.* **18** 3223